Article

Discovery Medicine 2025; 37(203): 3036–3050
https://doi.org/10.24976/Discov.Med.202537203.254

ANXA1 Treats Acute Aortic Dissection by Suppressing Macrophage Infiltration and NCF1-Induced Vascular Smooth Muscle Cell Apoptosis

Yingjian Ye[1], Qianqian Zhang[1], Guangwen Lu[1,*]

[1]Department of Emergency, The Third Affiliated Hospital of Wenzhou Medical University, 325200 Wenzhou, Zhejiang, China
*Correspondence: 13335772446@163.com (Guangwen Lu)
Submitted: 24 July 2025 Revised: 31 October 2025 Accepted: 3 November 2025 Published: 20 December 2025

Background: Acute aortic dissection (AAD) is a life-threatening cardiovascular disease with a high mortality rate. Macrophage infiltration and vascular smooth muscle cell (VSMC) apoptosis are crucial in AAD pathogenesis. However, Annexin A1 (ANXA1) may protect against AAD by mitigating aortic damage and cell apoptosis. Therefore, this study assesses the protective effects of ANXA1 in an Angiotensin II (Ang II)-induced AAD mouse model, focusing on survival rates, aortic structural integrity, and the mechanism underlying apoptosis in human aortic vascular smooth muscle cells (HAVSMCs) through regulation of M1 macrophages.

Methods: C57BL/6J mice (n = 40) were divided into four groups: the control group, ANXA1-treated group, Ang II-induced AAD group, and Ang II+ANXA1-treated group. The survival rate was monitored in AAD mice over a 28-day time point, and the diameters of the ascending aorta and aortic arch were evaluated by histological analysis. Immunohistochemistry (IHC) was used to examine cleaved caspase-3 levels in the thoracic aorta to assess VSMC apoptosis. *In vitro*, M1 macrophages were co-cultured with HAVSMCs. Immunofluorescence was performed to determine macrophage infiltration and oxidative stress by measuring F4/80 levels, Tetramethyl Rhodamine Ethyl Ester (TMRE) mitochondrial membrane potential, TdT-mediated dUTP Nick-End Labeling (TUNEL)-positive cells, and reactive oxygen species (ROS) levels in tissues and cells. Additionally, cleaved caspase-3 expression was evaluated both *in vivo* and *in vitro* using Western blot analysis to further assess VSMC apoptosis.

Results: ANXA1 exhibited significant protective effects in the Ang II-induced AAD mouse model. The survival rate in the Ang II+ANXA1 group was markedly higher than in the Ang II group ($p < 0.001$). The Ang II group had significantly dilated ascending aorta (AA) and aortic arch (Arch) compared to the Ang II+ANXA1 group ($p < 0.001$), whereas ANXA1 treatment did not alter aortic diameter in healthy mice. ANXA1 treatment substantially alleviated aortic dissection, intramural hematoma, and elastic fiber rupture in AAD mice. The Ang II+ANXA1 group has significantly reduced cleaved caspase-3 expression compared to the Ang II group ($p < 0.001$), indicating decreased VSMCs apoptosis. Furthermore, ANXA1 treatment reduced macrophage infiltration (F4/80 expression) and the number of Neutrophil Cytosolic Factor 1 (NCF1)-positive macrophages ($p < 0.001$). *In vitro* co-culture of HAVSMCs with M1 macrophages showed that ANXA1 substantially alleviated NCF1-positive cells, mitochondrial dysfunction, and apoptosis ($p < 0.001$). However, NCF1 upregulation in M1 macrophages effectively counteracted these effects.

Conclusions: In summary, ANXA1 protects against Ang II-induced AAD by improving survival rates, reducing vascular abnormalities, and preserving aortic structural integrity. It also inhibits vascular smooth muscle cell apoptosis, macrophage infiltration, and NCF1 expression. Mechanistically, ANXA1 reduces mitochondrial-dependent smooth muscle cell apoptosis by suppressing M1 macrophage-derived NCF1. These findings suggest ANXA1 has a potential therapeutic agent for AAD by targeting both inflammation and oxidative stress.

Keywords: acute aortic dissection; macrophage infiltration; vascular smooth muscle cell; Annexin A1; Neutrophil Cytosolic Factor 1

Introduction

Acute aortic dissection (AAD) is a life-threatening cardiovascular disease, defined by an intimal tear that allows blood to dissect between layers and create a false lumen [1–3]. This process leads to aortic dilation, disrupted perfusion, and ultimately aortic rupture. AAD development is closely associated with hypertension, arteriosclerosis, dysfunction of vascular smooth muscle cells (VSMCs), inflammation, oxidative stress, and apoptosis [4–6]. Although imaging has enhanced early diagnosis, there are still no effective treatments, and the mortality rate remains very high [7]. Therefore, understanding the underlying mechanisms and identifying novel therapeutic strategies remain addressed in the field of cardiovascular research.

Angiotensin II (Ang II) is a key mediator of hypertension and cardiovascular conditions [8–10]. It accelerates the progression of vascular injury by activating vaso-

constriction and promoting inflammatory signaling [11]. In AAD, Ang II triggers vascular smooth muscle cell apoptosis, endothelial dysfunction, and immune cell activation through its receptor, leading to structural disruption of the aortic wall [12,13]. Because Ang II-induced vascular damage is a crucial mechanism in the onset of AAD, Ang II-induced mouse models are commonly used to investigate disease mechanisms and to assess potential therapeutic approaches.

Annexin A1 (ANXA1), as an important cytokine, has been shown to play a crucial protective role across various cardiovascular diseases [14,15]. By interacting with membrane receptors, ANXA1 helps maintain membrane stability, reduces inflammation, inhibits apoptosis, and modulates immune responses [16,17]. Recent evidence indicates vascular advantages by reducing oxidative stress, inhibiting vascular smooth muscle cell (VSMC) apoptosis, and regulating macrophage polarization [17]. Furthermore, ANXA1 plays an anti-inflammatory and anti-apoptotic role in atherosclerosis and ischemic heart disease [18,19]. However, its role in AAD remains inadequately explored. Therefore, elucidating the ANXA1-mediated mechanisms in AAD may uncover novel therapeutic targets and guide new strategies for this disease.

Neutrophil Cytosolic Factor 1 (NCF1; $p47^{phox}$) is a critical cytoplasmic subunit of the NADPH oxidase complex that regulates the production of reactive oxygen species (ROS) [20,21]. Dysregulated NCF1 activity enhances vascular oxidative stress, endothelial dysfunction, and inflammatory responses, which are central mechanisms in the pathogenesis of aortic aneurysm and dissection [22,23]. Recent studies have demonstrated that upregulated NCF1 expression increases ROS accumulation, promotes macrophage activation, and induces vascular smooth muscle cell apoptosis, thereby compromising aortic wall integrity [24,25]. Given its central role in oxidative stress and vascular injury, NCF1 is recognized as a crucial mediator in AAD and represents a potential therapeutic target [26].

This study aims to investigate the protective role of ANXA1 in AAD by establishing an Ang II-induced AAD mouse model. The study assesses whether ANXA1 reduces mortality, alleviates aortic dilation and tissue injury, inhibits macrophage infiltration, and prevents vascular smooth muscle cell apoptosis in AAD mice. The findings are expected to support ANXA1 as a potential therapeutic candidate for AAD and to offer valuable insights into the development of clinical treatment strategies.

Materials and Methods

Animal Experiment

To establish the AAD-mouse model, 8-week-old male C57BL/6J mice (n = 40; HFK Bioscience, Beijing, China) were continuously injected with angiotensin II for 7 days. Mice were randomized into four groups, with 10 mice per group. The Ang II group was subcutaneously infused with angiotensin II (1 μg/kg/min) using an osmotic minipump for 4 days to induce AAD [27]. The control group was administered an equivalent volume of normal saline. The ANXA1 group received a daily intraperitoneal injection of recombinant ANXA1 protein (100 mg/kg). The Ang II+ANXA1 group received daily intraperitoneal injections of recombinant ANXA1 protein (100 mg/kg) in addition to the angiotensin II infusion. All surviving mice were euthanized at the common experimental endpoint (day 28) using sodium pentobarbital (110 mg/kg, i.p.), ensuring uniform sampling conditions.

After euthanasia, aortas were carefully examined to confirm the presence of AAD and then harvested for further analysis. For RNA and protein analysis, the ascending aorta (AA), aortic arch (Arch), and thoracic aorta (TA) were collected; for pathological analysis, only the TA was used. Tissue samples from mice that died during the experiment were collected immediately upon death and analyzed together with samples collected from survivors at the study endpoint.

All experimental procedures were approved by the Laboratory Animal Centre, South Zhejiang Institute of Radiation Medicine and Nuclear Technology Applications (Approval No. ZFY20250109).

Cell Culture

Human aortic vascular smooth muscle cells (HAVSMCs; 6110) were purchased from CELLRESEARCH (Shanghai, China) and were cultured in Smooth Muscle Cell Medium (SMCM; 1101, CELLRESEARCH, Shanghai, China).

For differentiation of M1 macrophages, THP-1 cells (SNL-044; SUNNCELL, Wuhan, Hubei, China) were cultured in RPMI-1640 medium supplemented with 10% FBS (RF medium). To generate M0 macrophages, THP-1 cells were induced with phorbol myristate acetate (PMA, 100 ng/mL) for 24 h in RF medium. Subsequently, M0 macrophages were polarized to M1 by culturing for 24 h in RF medium containing 1 ng/mL lipopolysaccharide (LPS) and 20 ng/mL interferon-γ (IFN-γ).

Phenotypic validations were performed using flow cytometry, confirming reduced cluster of differentiation 86 (CD86) and human leukocyte antigen – DR isotype (HLA-DR) expression in M0 cells and elevated CD86 and HLA-DR in M1 cells (**Supplementary Fig. 1**).

Indirect co-culture of HAVSMCs and M1 macrophages was performed as follows: THP-1 cells were differentiated into M1 macrophages (as described above) and seeded into the upper chamber of Transwell inserts (0.4 μm pore size). Cell cultures were maintained in RF medium containing reagents according to the experimental design, including Ang II (2.0 μM), recombinant ANXA1 protein (1.0 mM), and OE-NCF1 lentivirus. HAVSMCs were seeded in the lower chamber of the

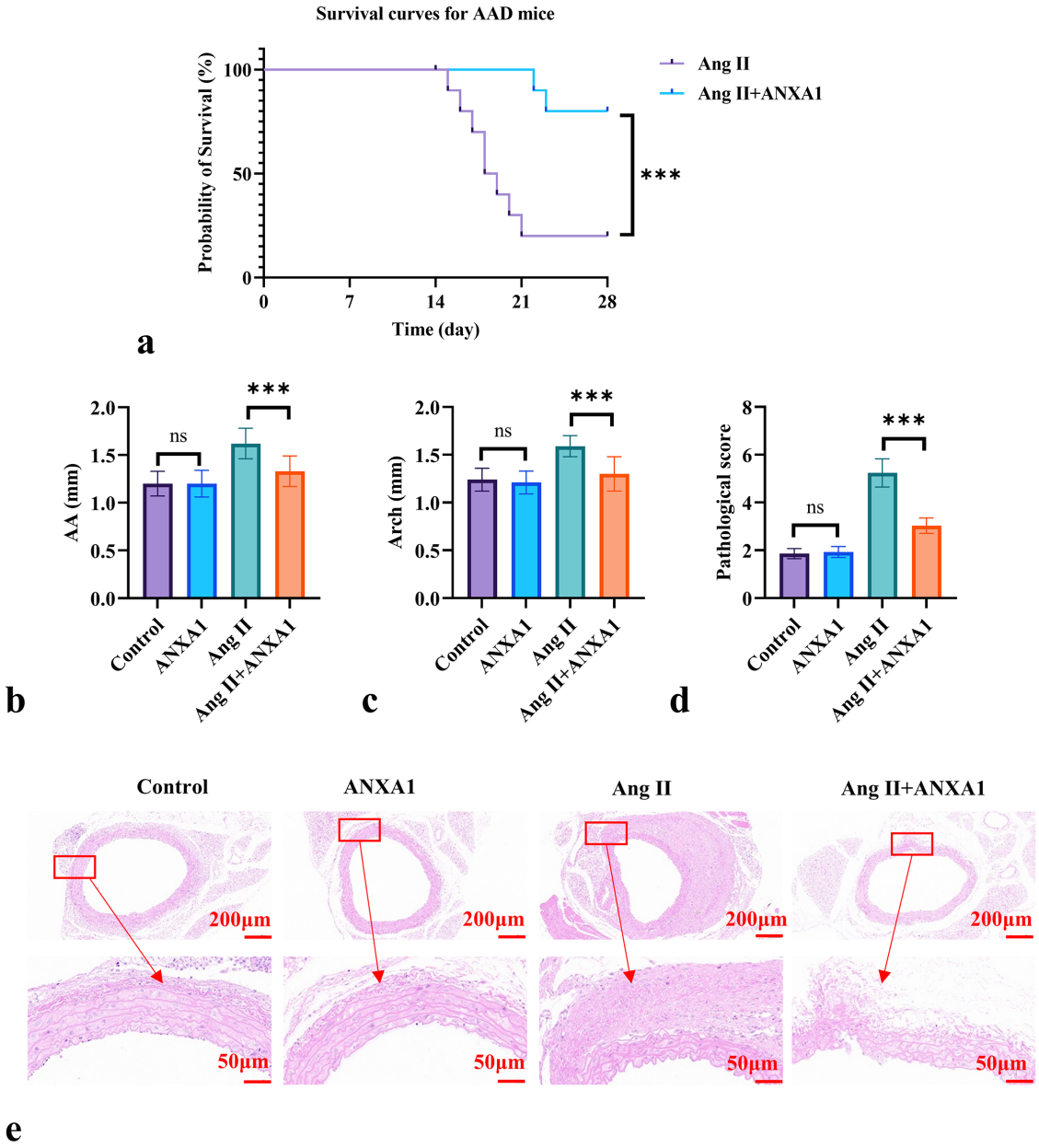

Fig. 1. Protective effect of ANXA1 in Ang II-induced AAD mouse model. (a) Survival curves of mice in the Ang II and Ang II+ANXA1 groups. AA and Arch diameters of mice in each group, photographed under a microscope at the end of the experiment. (b) AA values of mice in each group. (c) Arch values of mice. (d) Pathological scores derived from HE staining. (e) Representative images of the aortas (HE staining) from each group. n = 10. ns: not significant, ***$p < 0.001$. ANXA1, annexin A1; Ang II, angiotensin II; AAD, acute aortic dissection; AA, ascending aorta; Arch, aortic arch; HE, hematoxylin and eosin.

Transwell system. This setup allowed soluble factors secreted by M1 macrophages to influence HAVSMCs without direct cell-cell contact. All human cells were authenticated through STR profiling, and mycoplasma tests were negative.

Hematoxylin and Eosin (HE) Staining

Paraffin-embedded TA sections (4 μm) were initially incubated at 60 °C for 1 hour to enhance adhesion, then deparaffinized in xylene and rehydrated through graded ethanol (100%, 95%, 80%, 70%) and washed with distilled water. Nuclear staining was performed using hematoxylin for 5 minutes, briefly differentiated in 1% acid alcohol, and then rinsed under running tap water. Cytoplasm was coun-

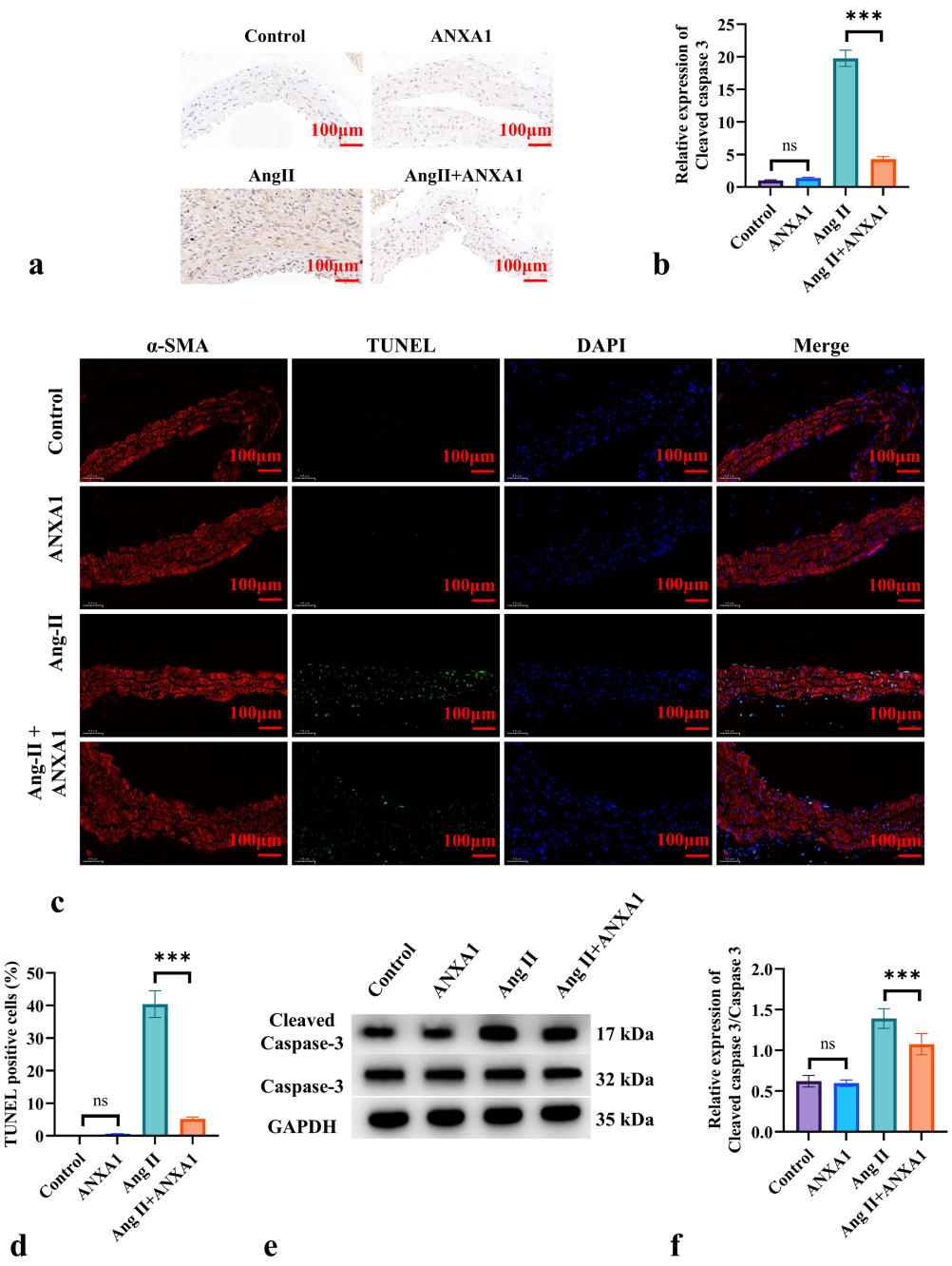

Fig. 2. ANXA1 alleviates VSMC apoptosis in the Ang II-induced AAD mouse model. (a,b) IHC analysis of cleaved caspase-3 expression in the aorta of mice from each group. (c,d) Immunofluorescence analysis of TUNEL-positive cells in the aorta from each group, with α-SMA labeling of VSMCs. (e,f) Western blot analysis of cleaved caspase-3 and caspase-3 protein expression in the aorta from each group. n = 10. ns: not significant, ***$p < 0.001$. VSMC, vascular smooth muscle cell; IHC, immunohistochemistry; TUNEL, TdT-mediated dUTP Nick-End Labeling.

terstained with eosin for 3 minutes. After staining, sections were dehydrated through increasing concentrations of ethanol, cleared in xylene, and mounted with a neutral resin medium. Finally, stained sections were examined and imaged using a light microscope (Leica DM750; Wetzlar, Germany).

Immunohistochemical (IHC) Assay

Aortic sections were dewaxed, rehydrated, subjected to antigen retrieval using an ethylenediaminetetraacetic acid (EDTA) solution, and treated to block endogenous peroxidase activity. The sections were incubated with primary antibody against cleaved caspase-3 (25128-1-AP, 1:1000,

Proteintech, Wuhan, China) for >16 h at 4 °C), and then underwent incubation with corresponding secondary antibody (ab6721, 1:1000, Abcam, Cambridge, UK) for >1 h in the dark. Subsequently, 3,3-diaminobenzidine (DAB) chromogen was added, and the sections were counterstained with HE. Finally, images were obtained using a Leica DM750 microscope (Wetzlar, Germany).

Immunofluorescence (IF) Assay

Immunofluorescence assay was used to evaluate F4/80 (ab300421, 1:1000, Abcam, Cambridge, UK), Alpha-Smooth Muscle Actin (α-SMA) (ab124964, 1:1000, Abcam, Cambridge, UK), and NCF1 (ab308256, 1:1000, Abcam, Cambridge, UK) in aortic samples and cultured cells. Tissue sections were dewaxed, rehydrated, and underwent antigen retrieval, and incubated with primary antibodies for >16 h at 4 °C, followed by treatment with the corresponding secondary antibody (ab150077, 1:500, Abcam, Cambridge, UK) for >2 h in the dark. Nuclei were counterstained with 4',6-diamidino-2-phenylindole (DAPI), and images were acquired on an ST5 laser confocal microscope (Leica, Wetzlar, Germany).

Cells cultured in confocal dishes were fixed with 4% formaldehyde for 20 min and permeabilized with 0.5% Triton™ X-100 for 60 min. Cells were then incubated with primary antibodies for >16 h at 4 °C, followed by incubation with corresponding secondary antibodies Alexa Fluor 488 (ab150077, 1:1000, Abcam, Cambridge, UK) and Alexa Fluor 647 (ab150079, 1:1000, Abcam, Cambridge, UK) for >2 h in the dark. Finally, nuclei were counterstained with DAPI, and images were obtained using an ST5 laser confocal microscope (Leica, Wetzlar, Germany).

Quantitative Reverse Transcription Polymerase Chain Reaction (qRT-PCR)

Total RNA was extracted from M1 macrophages using TRIzol reagent and from other cells using the Gene JET RNA Purification Kit, according to the manufacturer's instructions. Complementary DNA (cDNA) was synthesized using the iScript cDNA Synthesis Kit. qPCR was performed on a QuantStudio 6 Flex system (Thermo Scientific, Shanghai, China) using iTaq™ Universal SYBR Green Supermix. Relative mRNA expression was determined using the $2^{-\Delta\Delta Ct}$ method. Primers for qRT-PCR were synthesized by ThermoFisher Scientific (Waltham, MA, USA). Primer sequences are shown in Table 1.

Western Blot Analysis

Total proteins were extracted using radioimmunoprecipitation assay (RIPA) lysis buffer containing 1% of each protease inhibitor, phenylmethylsulfonyl fluoride, and super nuclease. For aortic tissues, samples were minced and suspended in RIPA lysis buffer. The mixture was homogenized using a tissue homogenizer (Roche, Shanghai, China), and the supernatants were collected. For cultured cells, pellets were resuspended in RIPA lysis buffer, shaken, and then centrifuged at 13,000 rpm for 20 min at 4 °C to collect the supernatant. Proteins were quantified using a bicinchoninic acid (BCA) assay.

Table 1. A list of primes used in qPCR.

Primes name	Primes sequences (5′-3′)
hum-*NCF1*-F	TGAGCCCAACTATGCAGGTG
hum-*NCF1*-R	CGTCTTGCCCTGACTTTTGC
hum-*GAPDH*-F	GTGGATATTGTTGCCATCAATGACC
hum-*GAPDH*-R	GCCCCAGCCTTCTTCATGGTGGT

NCF1, neutrophil cytosolic factor 1; *GAPDH*, glyceraldehyde-3-phosphate dehydrogenase.

Proteins were resolved on 12.5% sodium dodecyl sulfate-polyacrylamide gel electrophoresis (SDS-PAGE) and transferred to polyvinylidene difluoride (PVDF) membranes. After blocking with 5% skim milk for >2 h, membranes were trimmed by molecular weight and then incubated with primary antibodies against cleaved caspase-3 (1:1000, ab32042/ab214430, Abcam, Cambridge, UK), total caspase-3 (1:1000, ab184787, Abcam, Cambridge, UK), and glyceraldehyde-3-phosphate dehydrogenase (GAPDH) (1:1000, ab9485, Abcam, Cambridge, UK) at 4 °C for 18 h, followed by incubation with corresponding secondary antibodies (1:1000, ab6721, Abcam, Cambridge, UK) for 2 h. Protein bands were visualized using a 5800 multi-chemiluminescence imager (Tanon, Shanghai, China) and quantified with ImageJ (version 1.5f, National Institutes of Health, Bethesda, Maryland, USA, https://imagej.en.softonic.com/mac).

Cell Transfection

M1 macrophages were seeded in 96-well culture plates and incubated 24 hours before transfection to ensure a cell confluence of 50%–70%. Cell cultures were maintained overnight at 37 °C with 5% CO_2. For preparation of transfection complex, OE-NC plasmid or OE-NCF1 plasmid (sense: 5′-GAATTCATGGAGGAGGAGGAGGAGGAGGAGGAGGAGGAGGAGGAGGAGGAGGAGGAGGAGGAGGAGGAGGAGGAGGAGGAGGAGGAGGAGGAGGAGGAGGAGGAGGAGGAGGAGGAGGAGGAGGAGGAGGAGGAGGAGGAGGAGGAGGAGGAGGAGGAGGAGGAGGAGGAGGAGGAGGAGGAGGAGGAGGAGGAGGAGGAGGAGGAGGAGGAGGAGGAGGAGGAGGAGGAGGAGGAGGAGGAGGAGAGGAGGAGGAGGAGGAGGAGGAGGAGGAGGAGGAGGAGGAGGAGGAGTAACTCGAG-3′) (Sangon, Shanghai, China; 0.5 µg per well) were diluted in serum-free medium. Similarly, Lipofectamine 3000 was diluted in a separate tube using same serum free medium. DNA and transfection reagent solution were mixed and incubated at room temperature for 10–15 minutes to allow the DNA-transfection reagent complex formation. The com-

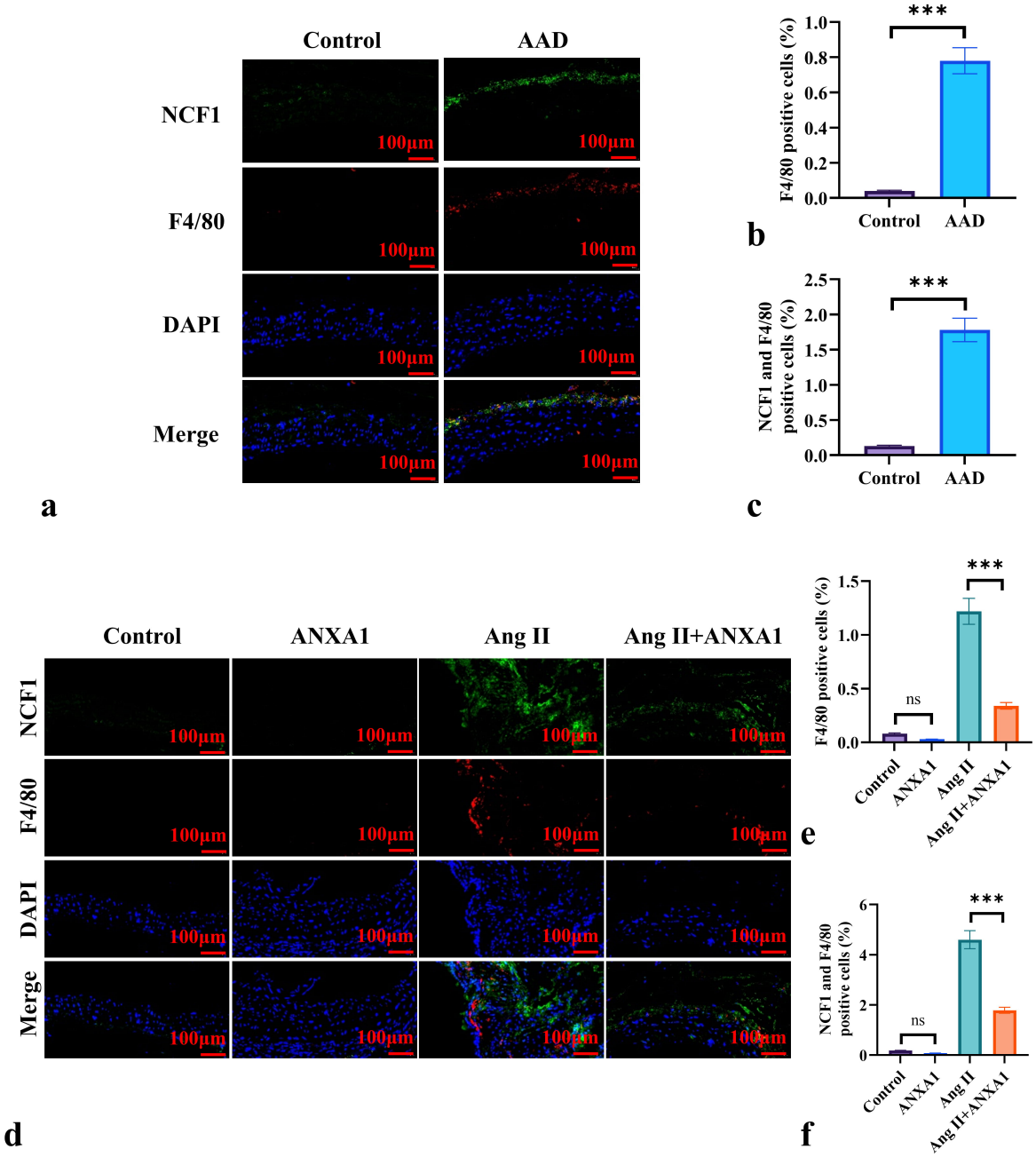

Fig. 3. ANXA1 reduces macrophage infiltration and NCF1 expression in AAD mice. (a–c) IF to detect the expression of F4/80 and NCF1 in the aorta of healthy and AAD mice. (d–f) IF to measure the expression of F4/80 and NCF1 in the aorta. "Positive cells (%)" indicates the ratio of marker-positive cells to total $DAPI^+$ nuclei. n = 10. ns: not significant, ***$p < 0.001$. NCF1, neutrophil cytosolic factor 1; IF, immunofluorescence; DAPI, 4',6-diamidino-2-phenylindole.

plex was gently added to the cultured cells and incubated for 4–6 hours at 37 °C with 5% CO_2. Culture medium was replaced with fresh complete medium and maintained under the same conditions for 48 hours. Finally, transfection efficiency was assessed using fluorescence microscopy and qRT-PCR.

Tetramethyl Rhodamine Ethyl Ester (TMRE) Assay

To evaluate mitochondrial membrane potential ($\Delta\Psi m$), cells were incubated with TMRE working solution (HY-D0985A, MCE, Monmouth Junction, NJ, USA) in pre-warmed culture medium at 37 °C for 25 minutes in the dark. Following staining, cells were gently rinsed with PBS to remove residual dye. Stained cells were examined under a fluorescence microscope (Leica, Wetzlar, Germany) using a TRITC-compatible filter set.

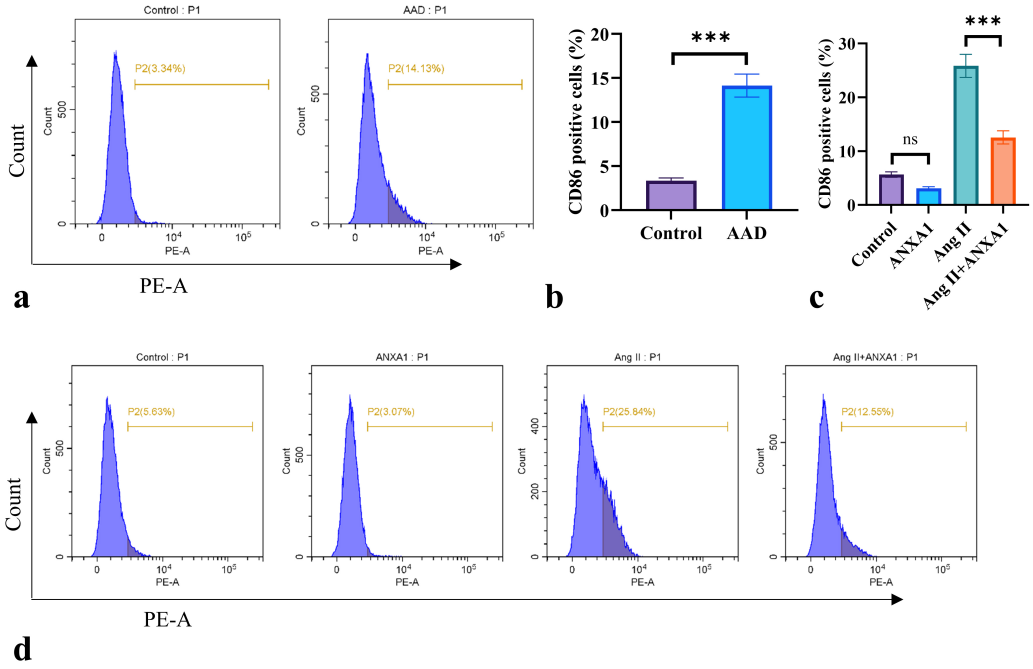

Fig. 4. ANXA1 reduces CD86 level in AAD mice. (a,b) Flow cytometry to detect the level of CD86 in the aorta of healthy and AAD mice. (c,d) Flow cytometry to measure the level of CD86 in the aorta. n = 10. ns: not significant, ***$p < 0.001$. CD86, cluster of differentiation 86.

TdT-Mediated dUTP Nick-End Labeling (TUNEL) Assay

Aortic sections were deparaffinized, rehydrated, and fixed with 4% formaldehyde, and then processed with the Click-iT™ Plus TUNEL Assay Kit (C10618/C10617) as follows: incubated with Proteinase K solution (15 min), TdT Reaction Buffer (10 min), TdT Reaction Mixture (60 min), 0.1% Triton™ X-100 (5 min), and the Click-iT™ Plus TUNEL Cocktail (30 min). Nuclei were counterstained with DAPI, and images were obtained using an ST5 laser confocal microscope (Leica, Wetzlar, Germany).

For cells, cultures in confocal dishes were fixed with 4% formaldehyde (30 min) and permeabilized with 0.3% Triton™ X-100 solution (5 min). Then, the TUNEL detection solution was applied for 60 min at 37 °C, followed by DAPI staining. Finally, images were acquired using an ST5 laser confocal microscope.

ROS Assay

Cells were seeded into culture plates and allowed to achieve 60%–80% confluence before treatment. Before staining, cells were washed twice with PBS, and the culture medium was discarded. The DCFH-DA stock solution (10 mM in DMSO) was freshly diluted to a 10 µM working solution and kept in the dark. The working solution was added to cover the cells, and the cells were incubated at 37 °C for 20 min, with gentle agitation to facilitate probe loading. After incubation, the staining solution was discarded, and the cells were washed three times with serum-free medium or PBS to remove excess probe. The cells were then fixed, stained with DAPI (1 µg/mL) for 5 min at room temperature in the dark, and washed twice with PBS. Images were acquired immediately using a fluorescence microscope with excitation at 488 nm and an emission at 525 nm. Fluorescence intensity was quantified using ImageJ or similar software.

Statistical Analysis

Statistical analyses were conducted using GraphPad Prism software (version 9.0, GraphPad Software, Inc., San Diego, CA, USA). Comparisons between two groups were performed using Student's *t*-tests, and comparisons in three or more groups were assessed using one-way Analysis of Variance (ANOVA) followed by Tukey's post-hoc test. A *p*-value of less than 0.05 was considered statistically significant.

Results

The Protective Effect of ANXA1 in the Ang II-Induced AAD Mouse Model

Over a 28-day timepoint, survival was monitored in AAD mice (Fig. 1a). The survival rate was significantly higher in the Ang II+ANXA1 group than in the Ang II group ($p < 0.001$). In the Ang II group, 10 mice developed AAD and 8 died. In the Ang II+ANXA1 group, 10 mice developed AAD and 2 died. Post-experiment assessment of the AA and Arch (Fig. 1b,c) revealed significantly greater diameters in the Ang II group than in the Ang II+ANXA1

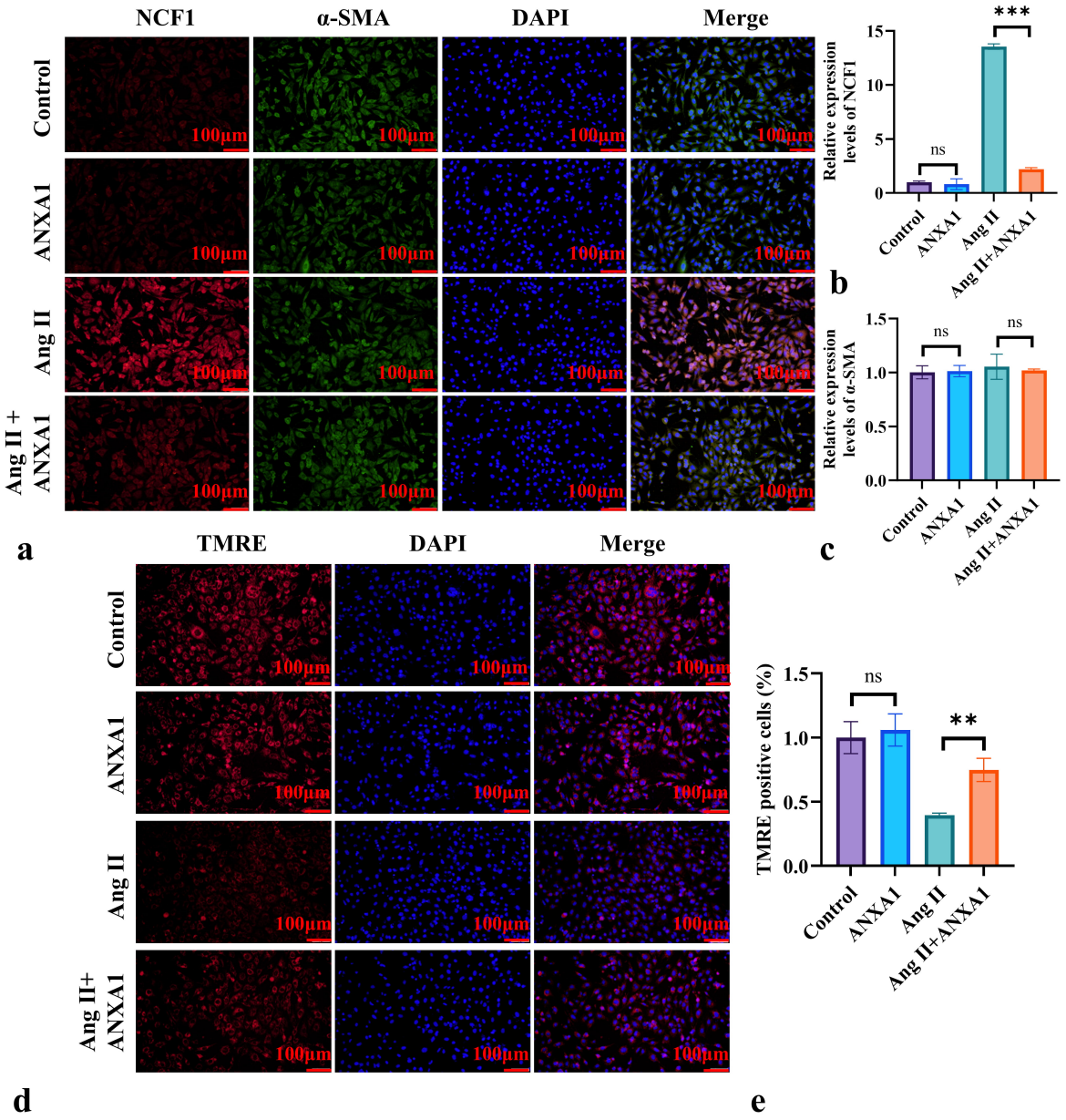

Fig. 5. ANXA1 mediates NCF1 expression and HAVSMC apoptosis. (a,b) Immunofluorescence staining to determine the proportion of NCF1-positive HAVSMCs after a 24-hour co-culture with M1 macrophages. (c) qRT-PCR to measure the NCF1 mRNA levels in HAVSMCs. (d,e) TMRE staining to determine the number of TMRE-positive HAVSMCs after a 24-hour co-culture. n = 6. ns: not significant, $^{**}p < 0.01$, $^{***}p < 0.001$. HAVSMCs, human aortic vascular smooth muscle cells; TMRE, Tetramethyl Rhodamine Ethyl Ester; α-SMA, Alpha-Smooth Muscle Actin.

group ($p < 0.001$). Compared to the control group, ANXA1 recombinant protein treatment alone did not alter AA and Arch diameters. Pathological scores obtained from HE staining are shown in Fig. 1d. As shown in Fig. 1e, the aortic architecture remained intact in both the control and ANXA1 groups. In contrast, the Ang II group exhibited intramural hematoma and rupture of elastic fibers, whereas the Ang II+ANXA1 group demonstrated only occasional elastic fiber rupture.

ANXA1 Alleviates VSMCs Apoptosis in Ang II-Induced AAD Mouse Model

The expression level of cleaved caspase 3 was notably higher in the Ang II group than in the Ang II+ANXA1 group ($p < 0.001$; Fig. 2a,b). Using α-SMA to label vascular smooth muscle cells (VSMCs), immunofluorescence staining revealed that Ang II-induced apoptotic cells were predominantly VSMCs. TUNEL staining indicated substantially greater VSMC apoptosis in the Ang II group than in the Ang II+ANXA1 group ($p < 0.001$; Fig. 2c,d). West-

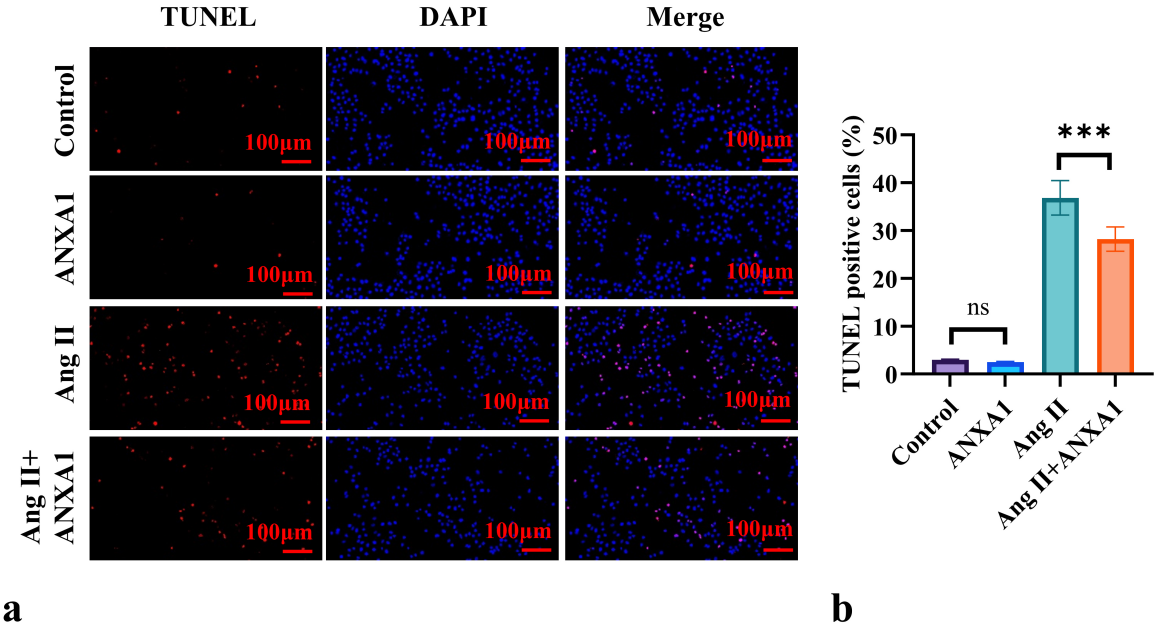

Fig. 6. ANXA1 mediates HAVSMC apoptosis. (a,b) TUNEL staining to measure the number of TUNEL-positive HAVSMCs after a 24-hour co-culture. n = 6. ns: not significant, ***$p < 0.001$.

ern blot analysis further showed a significantly elevated cleaved caspase-3/caspase 3 in the Ang II group compared to the Ang II+ANXA1 group ($p < 0.001$; Fig. 2e,f).

ANXA1 Alleviates Macrophage Infiltration and NCF1 Expression in AAD Mice

As illustrated in Fig. 3a,b, the AAD group had significantly higher F4/80 expression compared to the control group ($p < 0.001$), indicating greater macrophage infiltration. Additionally, the AAD group had more NCF1-positive macrophages than the control group ($p < 0.001$; Fig. 3c). Furthermore, immunofluorescence analysis revealed that ANXA1 regulates NCF1: both F4/80 and NCF1 expression levels were significantly higher in the Ang II group compared to the Ang II+ANXA1 group ($p < 0.001$), with marked co-localization of F4/80 and NCF1 (Fig. 3d–f).

Additionally, CD86-positive cells were significantly increased in the AAD group compared with the control group (Fig. 4a,b). Treatment with Ang II and ANXA1 substantially reduced CD86 positivity compared with Ang II alone ($p < 0.001$; Fig. 4c,d).

ANXA1 Alleviates HAVSMC Apoptosis by Suppressing the Expression of NCF1 in M1 Macrophages

In vitro, M1 macrophages were co-cultured with HAVSMCs and randomly divided into four intervention groups, followed by a 24-hour co-culture. After 24 hours, the number of NCF1-positive HAVSMCs was markedly lower in the Ang II+ANXA1 group than in the Ang II group ($p < 0.001$; Fig. 5a,b). In contrast, NCF1 mRNA expression level showed no significant difference between these two groups (Fig. 5c). There was a higher proportion of TMRE-positive cells in the Ang II+ANXA1 group than in the Ang II group ($p < 0.01$; Fig. 5d,e), indicating greater mitochondrial-dependent HAVSMC apoptosis in the Ang II group. Additionally, TUNEL staining showed fewer TUNEL-positive cells in the Ang II+ANXA1 group compared to the Ang II group ($p < 0.001$; Fig. 6a,b).

Furthermore, ROS levels in HAVSMCs were quantified and observed to be substantially higher in the Ang II group than in the Ang II+ANXA1 group ($p < 0.01$; Fig. 7a,b). Western blot analysis of cleaved caspase-3 and caspase-3 protein showed a significantly elevated cleaved caspase-3/caspase-3 in the Ang II group compared to the Ang II+ANXA1 group ($p < 0.001$; Fig. 7c,d).

To further explore whether ANXA1 inhibits VSMC apoptosis by suppressing NCF1 expression in M1 macrophages, VSMCs were transfected M1 macrophages with an NCF1 overexpression plasmid while maintaining Ang II and recombinant ANXA1 protein in the medium. Immunofluorescence showed that the NCF1 overexpression plasmid effectively increased the expression of NCF1 in M1 macrophages ($p < 0.001$; Fig. 8a,b), and qRT-PCR confirmed that the NCF1 overexpression plasmid was successfully transfected into M1 macrophages (Fig. 8c). After 24 h co-culture of transfected M1 macrophages with HAVSMCs (with Ang II and ANXA1 present in the medium), the number of NCF1-positive HAVSMCs was significantly increased in the OE-NCF1 group ($p < 0.001$), whereas NCF1 mRNA in HAVSMCs remained unchanged ($p > 0.05$; Fig. 8d–f). These observations suggest that NCF1 detected in HAVSMCs originates from M1 macrophages.

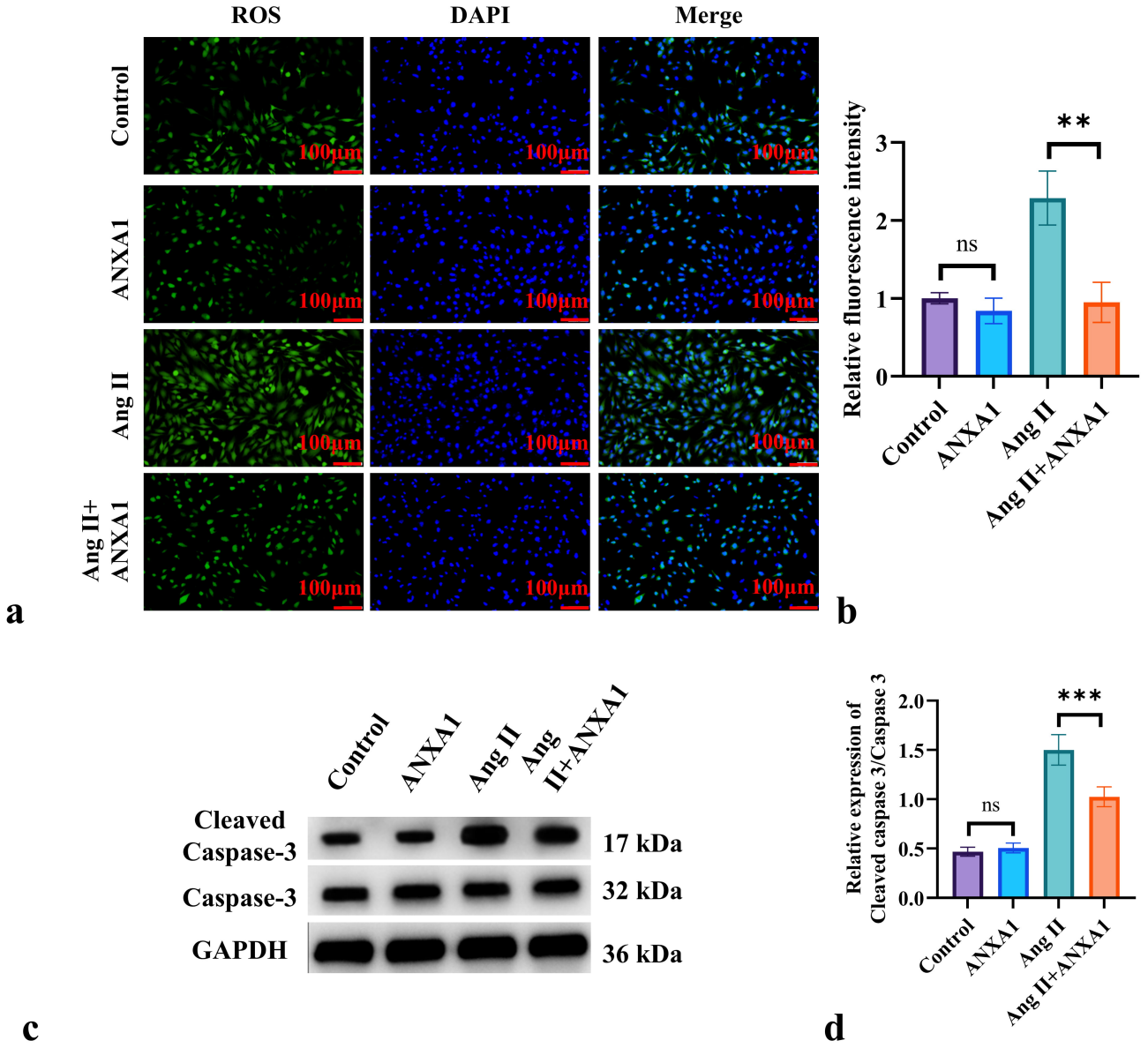

Fig. 7. ANXA1 mediates ROS production and cleaved caspase-3 protein expression in HAVSMCs. (a,b) Immunofluorescence staining to measure the ROS levels in HAVSMCs after co-culturing with M1 macrophages for 24 hours. (c,d) Western blot analysis to determine the expression of cleaved caspase-3 and caspase-3 proteins in HAVSMCs after a 24-hour co-culture. n = 6. ns: not significant, $^{**}p < 0.01$, $^{***}p < 0.001$. ROS, reactive oxygen species.

Subsequently, TMRE and TUNEL staining were performed to determine mitochondrial membrane potential and apoptosis in HAVSMCs, respectively. After a 24-hour co-culture, the OE-NCF1 group exhibited fewer TMRE-positive HAVSMCs than the OE-NC group ($p < 0.001$; Fig. 8g,h), and a higher proportion of TUNEL-positive cells ($p < 0.001$; Fig. 8i,j). Furthermore, the proportion of CD86-positive cells was significantly increased in the OE-NCF1 group compared with the OE-NC group ($p < 0.001$; Fig. 9a,b).

Moreover, ROS levels were also increased in the OE-NCF1 group than in the OE-NC group ($p < 0.001$; Fig. 10a,b). Western blot analysis (Fig. 10c,d) further confirmed a higher cleaved caspase-3/caspase-3 in the OE-NCF1 group ($p < 0.001$; Fig. 10c,d). Collectively, these findings indicate that ANXA1 inhibits mitochondrial-dependent HAVSMC apoptosis by downregulating NCF1 expression in M1 macrophages.

Discussion

This study first reveals that ANXA1 confers a significant protective effect in an Ang II-induced AAD mouse model, evidenced by lower mortality, reduced pathologic dilation of the AA and Arch, and minimization of aortic tissue damage. Mechanistic analysis showed that ANXA1

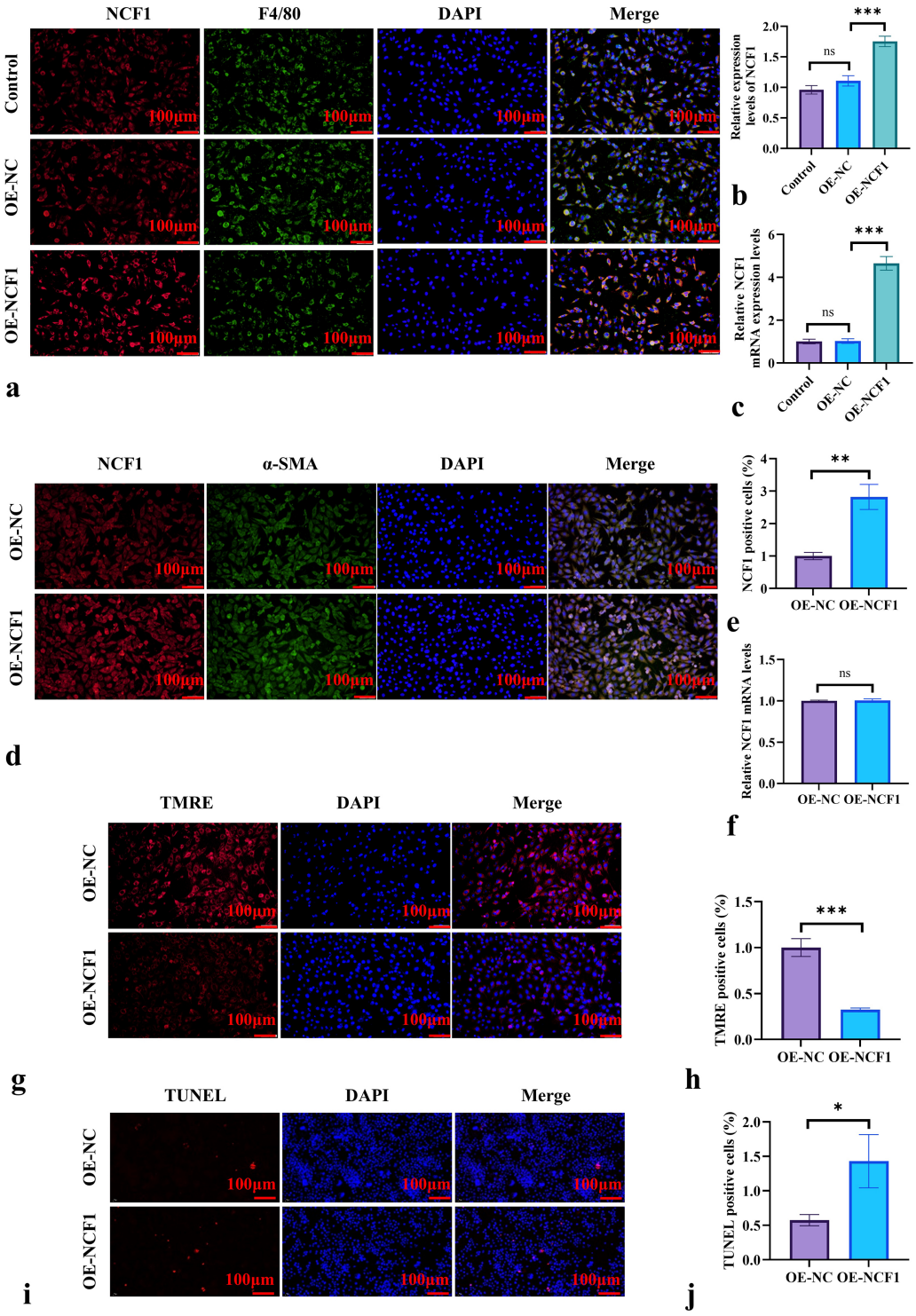

Fig. 8. ANXA1 alleviates HAVSMC apoptosis by inhibiting the expression of NCF1 in M1 macrophages. (a,b) After transfecting M1 macrophages with OE-NCF1, the cells were incubated with Ang II and recombinant ANXA1 protein for 24 hours, followed by IF to measure the number of NCF1-positive cells in M1 macrophages. (c) The transfection efficiency was confirmed using qRT-PCR. (d–f) After co-culturing HAVSMCs with transfected M1 macrophages for 24 hours, IF was used to measure the number of NCF1-positive HAVSMCs, and qRT-PCR was used to determine the mRNA level of NCF1 in HAVSMCs. (g,h) After a 24-hour co-culture, TMRE staining measured the number of TMRE-positive HAVSMCs. (i,j) After a 24-hour co-culture, TUNEL staining assessed the number of TUNEL-positive HAVSMCs. n = 6, ns: not significant, *$p < 0.05$, **$p < 0.01$, ***$p < 0.001$. OE-NCF1, overexpression of NCF1.

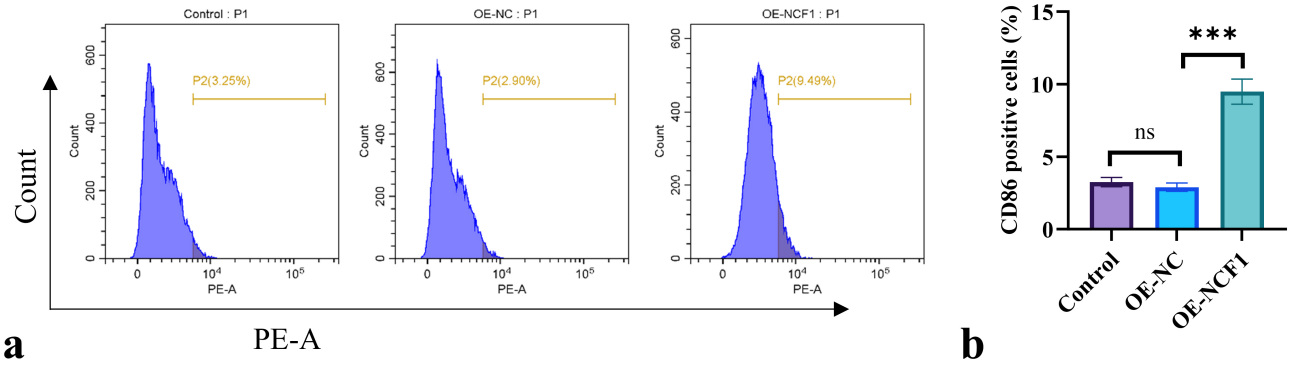

Fig. 9. ANXA1 alleviates HAVSMC apoptosis by inhibiting the expression of NCF1 in M1 macrophages. (a,b) After a 24-hour co-culture, the number of CD86-positive HAVSMCs was determined using flow cytometry. n = 6. ns: not significant, ***$p < 0.001$.

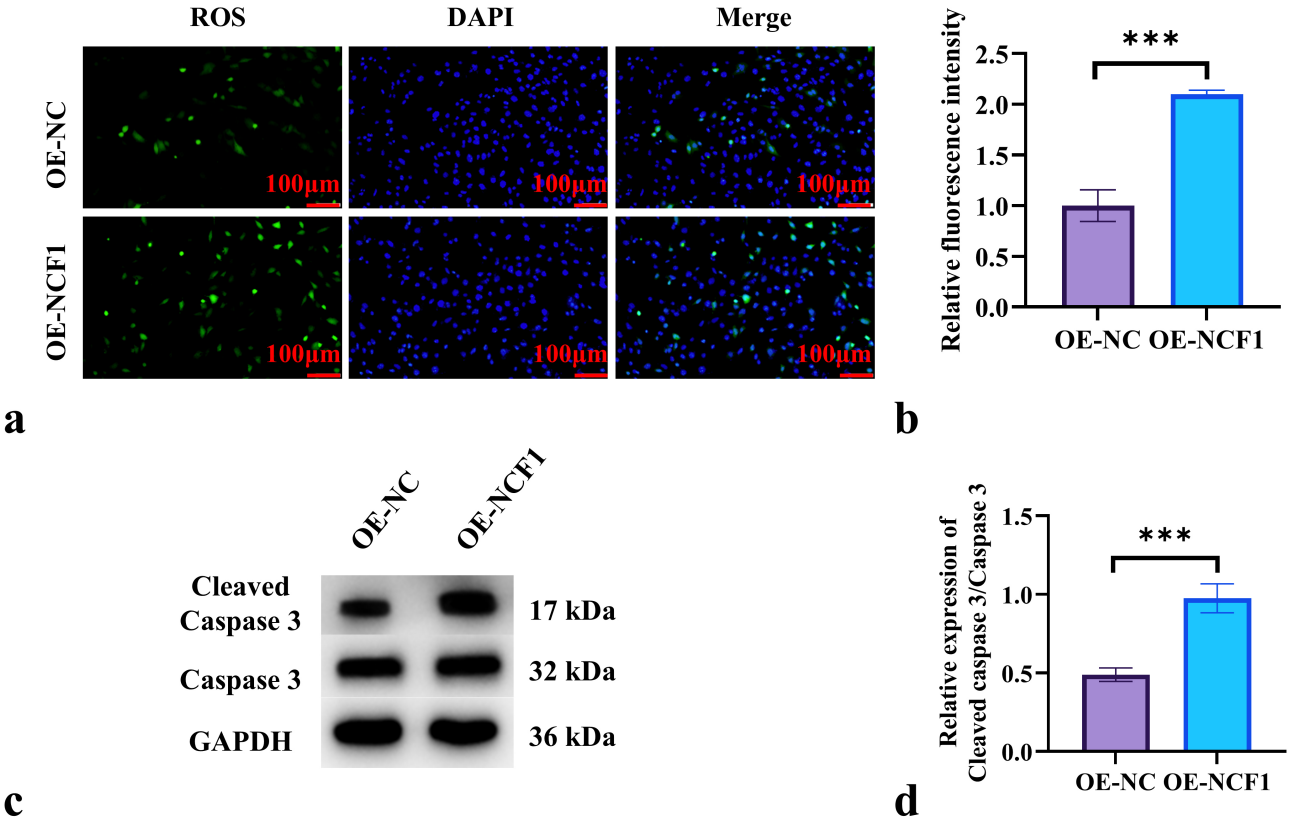

Fig. 10. ANXA1 inhibits the expression of NCF1 in M1 macrophages to alleviate ROS levels and cleaved caspase-3 expression in HAVSMCs. (a,b) After co-culturing HAVSMCs with M1 macrophages transfected with OE-NCF1 for 24 hours, fluorescence staining was used to measure ROS levels in HAVSMCs. (c,d) After a 24-hour co-culture, Western blotting measured the protein expression of cleaved caspase-3 and caspase-3 in HAVSMCs. n = 6. ***$p < 0.001$.

mitigates AAD by inhibiting macrophage infiltration, reducing oxidative stress, and suppressing VSMCs apoptosis. These observations are consistent with prior findings of ANXA1's anti-inflammatory and anti-apoptotic roles, providing new insights into vascular pathology and highlighting its therapeutic potential [20,21].

Our survival analysis demonstrated a substantially higher survival rate of the Ang II+ANXA1 group than the Ang II group. This observation aligns with previous evidence of ANXA1's cardioprotective roles, including anti-apoptotic and anti-inflammatory effects in models of atherosclerosis and myocardial ischemia [14,22]. Moreover, ANXA1 treatment did not alter AA and Arch diameters in healthy mice, further suggesting that its protective role is specific to pathological conditions and does not interfere with normal tissue structure [23].

Histologically, HE staining showed significant elastic fiber rupture and hematoma formation in the Ang II group,

whereas mice in the Ang II+ANXA1 group exhibited only occasional elastic fiber damage. These results support the structural protective role of ANXA1 in the vascular wall and align with previous studies that ANXA1 reduces tissue damage by modulating the inflammatory response [24]. The findings further indicate that ANXA1 not only inhibits systemic aortic dilation but also directly alleviates local tissue damage.

In further experiments evaluating VSMC apoptosis, Ang II-induced AAD mice demonstrated a significant increase in cleaved caspase-3, whereas ANXA1 effectively inhibited this apoptotic pathway. TUNEL assay and α-SMA co-staining further showed that Ang II significantly increased VSMC apoptosis, which was substantially reduced by ANXA1. These results align with earlier findings that ANXA1 inhibits apoptosis by reducing caspase-3 activity [25]. Altogether, the results suggest that ANXA1 supports VSMC survival through multiple pathways, thereby alleviating aortic wall damage during AAD pathogenesis.

At the same time, we also found that ANXA1 plays a crucial role in regulating macrophage infiltration and their oxidative stress response in AAD. Immunofluorescence analysis showed a substantial rise in macrophage infiltration in the AAD group, accompanied by increased NCF1 expression in macrophages. Given that NCF1 is a key regulator of oxidative stress and is closely associated with the progression of various cardiovascular diseases [26,28], these results show increased oxidative signaling in AAD. Notably, the Ang II+ANXA1 group demonstrated substantially reduced macrophage infiltration and decreased NCF1 expression, indicating that ANXA1 inhibits macrophage activation and oxidative stress. This is consistent with earlier findings that ANXA1 modulates macrophage polarization and function [14]. The inhibitory effects on macrophage infiltration may be due to ANXA1-mediated shift between M1 and M2 phenotypes, as reported in other inflammatory models [29].

In vitro co-culture of M1 macrophages with HAVSMCs further confirmed that ANXA1 alleviates VSMC mitochondrial apoptosis by inhibiting NCF1 expression in M1 macrophages. Compared to the Ang II-only treatment group, the Ang II+ANXA1 group showed a significant reduction in NCF1 expression in HAVSMCs. TMRE and TUNEL assays indicated that ANXA1 preserves mitochondrial membrane potential and reduces apoptosis in HAVSMCs. These results indicate that ANXA1 alleviates Ang II-induced vascular damage by regulating macrophage-smooth muscle cell interactions [19,30].

Although our study demonstrates several promising outcomes, we acknowledge certain limitations. First, the animal sample size was relatively small, and the Ang II-induced AAD model used younger mice, which may limit generalizability to human disease. Second, the cellular source of NCF1 was not definitively established, and loss-of-function experiments were not performed to confirm its role. Third, we did not evaluate other inflammatory mediators or signaling pathways that may be modulated by ANXA1, and the *in vitro* assays may not fully recapitulate the *in vivo* environment. While our findings support a protective role for ANXA1 in AAD, further larger studies and comprehensive mechanistic investigations are warranted.

In conclusion, this study reveals the protective role of ANXA1 in the Ang II-induced AAD mouse model by limiting aortic dilation and tissue damage through reduced macrophage infiltration, suppression of VSMC apoptosis, and alleviation of oxidative stress. These observations provide experimental evidence for ANXA1 as a potential therapeutic candidate for AAD and underscore macrophage-VSMC interaction as a valuable target for intervention. Future studies should explore ANXA1 in additional vascular disease models and elucidate its molecular regulatory mechanisms.

Conclusions

In summary, ANXA1 exerts protective effects in Ang II-induced AAD by significantly improving survival rates, reducing dilation of the ascending aorta and aortic arch, and preserving aortic structural integrity. It also mitigates VSMC apoptosis, decreases macrophage infiltration, and lowers NCF1 expression. Mechanistically, ANXA1 suppresses M1 macrophage-derived NCF1 expression, thereby inhibiting mitochondrial-dependent apoptosis in VSMCs. These results support the notion that ANXA1 could be a potential therapeutic candidate for treating AAD, targeting both inflammatory and oxidative stress pathways.

Availability of Data and Materials

All data generated or analyzed during this study are included in this published article and its supplementary material. Additional raw data are available from the corresponding author upon reasonable request.

Author Contributions

GL contributed to conceptualization, methodology, supervision, and project administration. QZ contributed to data curation, formal analysis, investigation, visualization, and drafting of the original manuscript. YY contributed to conceptualization, methodology, data curation, formal analysis, investigation, visualization, and drafting of the original manuscript. All authors have been involved in revising it critically for important intellectual content. All authors approved the final version of the manuscript, and agreed to be accountable for all aspects of the work to ensure that questions related to accuracy or integrity are appropriately investigated and resolved.

Ethics Approval and Consent to Participate

All animal experiments were approved by the Experimental Animal Center of the South Zhejiang Institute of Radiation Medicine and Nuclear Technology Applications (Approval No. ZFY20250109). All procedures were carried out in accordance with institutional ethical guidelines, with efforts made to minimize animal use and suffering.

Acknowledgment

Not applicable.

Funding

This research received no external funding.

Conflict of Interest

The authors declare no conflict of interest.

Supplementary Material

Supplementary material associated with this article can be found, in the online version, at https://doi.org/10.24976/Discov.Med.202537203.254.

References

[1] Sorber R, Hicks CW. Diagnosis and Management of Acute Aortic Syndromes: Dissection, Penetrating Aortic Ulcer, and Intramural Hematoma. Current Cardiology Reports. 2022; 24: 209–216. https://doi.org/10.1007/s11886-022-01642-3.

[2] Sayed A, Munir M, Bahbah EI. Aortic Dissection: A Review of the Pathophysiology, Management and Prospective Advances. Current Cardiology Reviews. 2021; 17: e230421186875. https://doi.org/10.2174/1573403X16666201014142930.

[3] Reed MJ. Diagnosis and management of acute aortic dissection in the emergency department. British Journal of Hospital Medicine. 2024; 85: 1–9. https://doi.org/10.12968/hmed.2023.0366.

[4] Liu H, Li H, Han L, Zhang Y, Wu Y, Hong L, *et al*. Inflammatory risk stratification individualizes anti-inflammatory pharmacotherapy for acute type A aortic dissection. Innovation. 2023; 4: 100448. https://doi.org/10.1016/j.xinn.2023.100448.

[5] Zhang B, Zeng K, Guan RC, Jiang HQ, Qiang YJ, Zhang Q, *et al*. Single-Cell RNA-Seq Analysis Reveals Macrophages Are Involved in the Pathogenesis of Human Sporadic Acute Type A Aortic Dissection. Biomolecules. 2023; 13: 399. https://doi.org/10.3390/biom13020399.

[6] Song W, Chen Y, Qin L, Xu X, Sun Y, Zhong M, *et al*. Oxidative stress drives vascular smooth muscle cell damage in acute Stanford type A aortic dissection through HIF-1α/HO-1 mediated ferroptosis. Heliyon. 2023; 9: e22857. https://doi.org/10.1016/j.heliyon.2023.e22857.

[7] Chen J, Bai Y, Liu H, Qin M, Guo Z. Prediction of in-hospital death following acute type A aortic dissection. Frontiers in Public Health. 2023; 11: 1143160. https://doi.org/10.3389/fpubh.2023.1143160.

[8] Lagrange J, Finger S, Kossmann S, Garlapati V, Ruf W, Wenzel P. Angiotensin II Infusion Leads to Aortic Dissection in LRP8 Deficient Mice. International Journal of Molecular Sciences. 2020; 21: 4916. https://doi.org/10.3390/ijms21144916.

[9] Wu XW, Li G, Cheng XB, Wang M, Wang LL, Wang HH, *et al*. Association of Angiotensin II Type 1 Receptor Agonistic Autoantibodies With Outcomes in Patients With Acute Aortic Dissection. JAMA Network Open. 2021; 4: e2127587. https://doi.org/10.1001/jamanetworkopen.2021.27587.

[10] Shen L, Li F, Xia K, Zhan L, Zhang D, Yan Z. Nuclear receptor subfamily 4 group a member 1 eases angiotensin II-arose oxidative stress in vascular smooth muscle cell by boosting nucleotide-binding oligomerization domain-like receptor family caspase recruitment domain containing 3 transcription. CytoJournal. 2024; 21: 43. https://doi.org/10.25259/Cytojournal_86_2024.

[11] Vandestienne M, Zhang Y, Santos-Zas I, Al-Rifai R, Joffre J, Giraud A, *et al*. TREM-1 orchestrates angiotensin II-induced monocyte trafficking and promotes experimental abdominal aortic aneurysm. The Journal of Clinical Investigation. 2021; 131: e142468. https://doi.org/10.1172/JCI142468.

[12] Kondapalli NB, Katari V, Dalal K, Paruchuri S, Thodeti CK. Angiotensin II induces endothelial dysfunction and vascular remodeling by downregulating TRPV4 channels. Journal of Molecular and Cellular Cardiology Plus. 2023; 6: 100055. https://doi.org/10.1016/j.jmccpl.2023.100055.

[13] Liu G, Chen Y, Wang Y, Deng X, Xiao Q, Zhang L, *et al*. Angiotensin II enhances group 2 innate lymphoid cell responses via AT1a during airway inflammation. The Journal of Experimental Medicine. 2022; 219: e20211001. https://doi.org/10.1084/jem.20211001.

[14] Xu X, Gao W, Li L, Hao J, Yang B, Wang T, *et al*. Annexin A1 protects against cerebral ischemia-reperfusion injury by modulating microglia/macrophage polarization via FPR2/ALX-dependent AMPK-mTOR pathway. Journal of Neuroinflammation. 2021; 18: 119. https://doi.org/10.1186/s12974-021-02174-3.

[15] Zhou H, Yan L, Huang H, Li X, Xia Q, Zheng L, *et al*. Tat-NTS peptide protects neurons against cerebral ischemia-reperfusion injury via ANXA1 SUMOylation in microglia. Theranostics. 2023; 13: 5561–5583. https://doi.org/10.7150/thno.85390.

[16] Novizio N, Belvedere R, Pessolano E, Morello S, Tosco A, Campiglia P, *et al*. ANXA1 Contained in EVs Regulates Macrophage Polarization in Tumor Microenvironment and Promotes Pancreatic Cancer Progression and Metastasis. International Journal of Molecular Sciences. 2021; 22: 11018. https://doi.org/10.3390/ijms222011018.

[17] Qin S, Ren YC, Liu JY, Chen WB, Fu B, Zheng J, *et al*. ANXA1sp attenuates sepsis-induced myocardial injury by promoting mitochondrial biosynthesis and inhibiting oxidative stress and autophagy via SIRT3 upregulation. The Kaohsiung Journal of Medical Sciences. 2024; 40: 35–45. https://doi.org/10.1002/kjm2.12767.

[18] Shen X, Zhang S, Guo Z, Xing D, Chen W. The crosstalk of ABCA1 and ANXA1: a potential mechanism for protection against atherosclerosis. Molecular Medicine. 2020; 26: 84. https://doi.org/10.1186/s10020-020-00213-y.

[19] Chen J, Oggero S, Cecconello C, Dalli J, Hayat H, Hjiej Andaloussi A, *et al*. The Annexin-A1 mimetic RTP-026 promotes acute cardioprotection through modulation of immune cell activation. Pharmacological Research. 2023; 198: 107005. https://doi.org/10.1016/j.phrs.2023.107005.

[20] You Q, Ke Y, Chen X, Yan W, Li D, Chen L, *et al*. Loss of Endothelial Annexin A1 Aggravates Inflammation-Induched Vascular Aging. Advanced Science. 2024; 11: e2307040. https://doi.org/10.1002/advs.202307040.

[21] Zheng Y, Li Y, Li S, Hu R, Zhang L. Annexin A1 (Ac2-26)-dependent Fpr2 receptor alleviates sepsis-induced acute kidney injury by inhibiting inflammation and apoptosis in vivo and in

vitro. Inflammation Research. 2023; 72: 347–362. https://doi.org/10.1007/s00011-022-01640-9.

[22] Liao WI, Wu SY, Tsai SH, Pao HP, Huang KL, Chu SJ. 2-Methoxyestradiol Protects Against Lung Ischemia/Reperfusion Injury by Upregulating Annexin A1 Protein Expression. Frontiers in Immunology. 2021; 12: 596376. https://doi.org/10.3389/fimmu.2021.596376.

[23] Wu L, Liu C, Chang DY, Zhan R, Sun J, Cui SH, *et al*. Annexin A1 alleviates kidney injury by promoting the resolution of inflammation in diabetic nephropathy. Kidney International. 2021; 100: 107–121. https://doi.org/10.1016/j.kint.2021.02.025.

[24] de Araújo S, de Melo Costa VR, Santos FM, de Sousa CDF, Moreira TP, Gonçalves MR, *et al*. Annexin A1-FPR2/ALX Signaling Axis Regulates Acute Inflammation during Chikungunya Virus Infection. Cells. 2022; 11: 2717. https://doi.org/10.3390/cells11172717.

[25] Xia Q, Mao M, Zeng Z, Luo Z, Zhao Y, Shi J, *et al*. Inhibition of SENP6 restrains cerebral ischemia-reperfusion injury by regulating Annexin-A1 nuclear translocation-associated neuronal apoptosis. Theranostics. 2021; 11: 7450–7470. https://doi.org/10.7150/thno.60277.

[26] Liu H, Yang P, Chen S, Wang S, Jiang L, Xiao X, *et al*. Ncf1 knockout in smooth muscle cells exacerbates angiotensin II-induced aortic aneurysm and dissection by activating the STING pathway. Cardiovascular Research. 2024; 120: 1081–1096. https://doi.org/10.1093/cvr/cvae081.

[27] Ito S, Hashimoto Y, Majima R, Nakao E, Aoki H, Nishihara M, *et al*. MRTF-A promotes angiotensin II-induced inflammatory response and aortic dissection in mice. PLoS ONE. 2020; 15: e0229888. https://doi.org/10.1371/journal.pone.0229888.

[28] Li M, Xin S, Gu R, Zheng L, Hu J, Zhang R, *et al*. Novel Diagnostic Biomarkers Related to Oxidative Stress and Macrophage Ferroptosis in Atherosclerosis. Oxidative Medicine and Cellular Longevity. 2022; 2022: 8917947. https://doi.org/10.1155/2022/8917947.

[29] Pearanpan L, Nordin FJ, Siew EL, Kumolosasi E, Mohamad Hanif EA, Masre SF, *et al*. A Cell-Based Systematic Review on the Role of Annexin A1 in Triple-Negative Breast Cancers. International Journal of Molecular Sciences. 2022; 23: 8256. https://doi.org/10.3390/ijms23158256.

[30] Ries M, Watts H, Mota BC, Lopez MY, Donat CK, Baxan N, *et al*. Annexin A1 restores cerebrovascular integrity concomitant with reduced amyloid-β and tau pathology. Brain. 2021; 144: 1526–1541. https://doi.org/10.1093/brain/awab050.